JMEPEG (2022) 31:7204–7219
https://doi.org/10.1007/s11665-022-06761-0

1059-9495/$19.00

TECHNICAL ARTICLE

Isoxazoline Derivatives as Inhibitors for Mild Steel Corrosion in 1M H_2SO_4: Computational and Experimental Investigations

N. Anusuya, J. Saranya, F. Benhiba, I. Warad, A. Zarrouk, and S. Chitra

Submitted: 8 August 2021 / Revised: 4 December 2021 / Accepted: 29 January 2022 / Published online: 16 March 2022

The isoxazoline derivatives namely 3-phenylamino-5-(3′-methoxy-4′-hydroxyphenyl) isoxazoline (PAMHI), 3-phenylamino-5-(4′-methoxyphenyl)isoxazoline (PAMI) and 3-phenylamino-5-(4′-hydroxyphenyl)isoxazoline (PAHI) were synthesized and tested for their inhibition capacity against the mild steel (MS) corrosion in 1 M H_2SO_4. Their inhibition performance toward MS has been studied through well-known methods namely weight loss (WL), electrochemical and surface analysis. The inhibition efficiency of PAMHI was 95.90% at 10mM concentration. The adsorption studies indicated that the isoxazoline derivatives obeyed Langmuir adsorption isotherm on the mild steel surface, and Gibbs free energy values were in the range of -32.05, -28.52 and -33.44 kJ mol^{-1}. These results suggested that the inhibitor molecules interacted with the mild steel surface through mixture adsorption. Also, mixed type behavior was observed for the studied inhibitors from polarization studies. The presence of a protective layer of organic matter was validated by scanning electron microscopy (SEM) and atomic force microscopy (AFM) techniques. Density-functional theory (DFT) method and molecular dynamics (MD) simulation have been studied and the results shown that the inhibitory efficiencies of the three molecules tested are almost the same.

Graphical Abstract

Molecular structure of the inhibitors

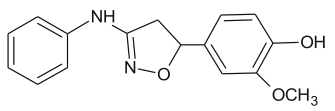

3-phenylamino-5-(3′-methoxy-4′-hydroxyphenyl)isoxazoline (PAMHI)

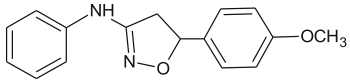

3-phenylamino-5-(4′-methoxyphenyl)isoxazoline (PAMI)

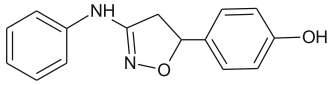

3-phenylamino-5-(4′-hydroxyphenyl)isoxazoline (PAHI)

N. Anusuya and **S. Chitra**, Department of Chemistry, PSGR Krishnammal College for Women, Coimbatore, India; **J. Saranya**, Department of Humanities and Sciences (Chemistry), Gokaraju Rangaraju Institute of Engineering and Technology, Hyderabad, India; **F. Benhiba**, Laboratory of Separation Processes, Faculty of Sciences, Ibn Tofail University, PO Box 133, 14000 Kenitra, Morocco; and Laboratory of Materials, Nanotechnology and Environment, Faculty of Sciences, Mohammed V University in Rabat, Av. Ibn Battouta, P.O. Box. 1014, Agdal-Rabat, Morocco; **I. Warad**, Department of Chemistry, AN-Najah National University, P.O. Box 7, Nablus, Palestine; and **A. Zarrouk**, Laboratory of Materials, Nanotechnology and Environment, Faculty of Sciences, Mohammed V University in Rabat, Av. Ibn Battouta, P.O. Box. 1014, Agdal-Rabat, Morocco. Contact e-mails: jcsaranya.chem96@gmail.com azarrouk@gmail.com.

Keywords DFT, isoxazolines, mild steel corrosion, molecular dynamic simulation, SEM/AFM

1. Introduction

Corrosion is a natural process which results from physicochemical interactions between a metal and its environment that leads to a weakening of the metal surface, its surroundings and that could affect the technical systems of which they make a part of it. Generally, the resistance of the material depends upon the surrounding environment and of course is not an

intrinsic property. Corrosion can be controlled by proper selection of the materials and an irrational control of the chemical composition of the environment. Corrosion affects the world's economy, people's health and safety like how corona in these two years affecting the entire world. Almost in all industries, mild steel (MS) is a common and cheap metal used because of its good mechanical, physical and chemical properties. The ferromagnetic properties of MS make it more perfect for the manufacture of electrical devices and motors. Nearly most of the industries are extensively using sulfuric acid medium as corrosive solution, which induced a great deal of research on MS (Ref 1). The deterioration of the metal caused by this medium makes the research more anticipated toward the use of corrosion inhibitors (Ref 2). Though many corrosion controlling methods are available, application of inhibitors to acidic medium was found to be effective in industries like electroplating, boilers, energy, etc. In these industries, corrosion occurs during acid pickling, descaling, etc., because these processes are taking place frequently.

In past few decades, organic inhibitors are more preferred due to environment safety and also they perform well in almost all environments. Moreover, corrosion inhibitors that are usually operative only for specific metal/alloys in some environment, but the rust environments are vastly variable; thus, an inhibitor may not work well in all the environments. So, it is required to develop and design new compounds that can act well for different environment and plentiful compounds are designed (Ref 3). Compounds containing nitrogen, oxygen, phosphorous, π-bonds, etc., are considered to be active corrosion inhibitors (Ref 3, 4) and the molecules get adsorbed on the metal surface via adsorption phenomenon; thereby creates a barrier to corrodent attack. Physicochemical properties such as aromaticity, functional groups, molecular size, molecular weight, steric factor, molecular structure, orbital character of donating π electrons and electron density of the donor atoms are mainly responsible for adsorption process.

In this context, many researchers have studied a variety of compounds containing heterocycles in their structure (Ref 5-8). Recently, the carbon dot inhibitors have been reported in order to replace the conventional inhibitors and to avoid environmental pollution (Ref 9, 10). Among the organic inhibitors reported so far, the isoxazoline derivatives were selected for this study based on the fact that they are five membered organic structures that contain oxygen and nitrogen heteroatoms which are mainly responsible for corrosion inhibition. Substituted isoxazoline derivatives find an extensive range of applications in the field of pharmaceutical, agrochemical agents and medicinal research. These are also used as corrosion inhibitors for fuels and lubricants and show good potency in animal lubricants (Ref 11, 12).

N&O-containing azole heterocyclic molecules possess lone pair of electrons on the oxygen and nitrogen atoms that have beneficial effects that are related to their special affinity to adsorb on the metallic surfaces. These lone pair of electrons can interact favorably with the vacant orbitals of metal, leading to the formation of protective barrier film. Only 7% of the papers have been reported on the isoxazole derivatives so far (Ref 13). These properties expressed their antitoxic environment and eco-friendly. These compounds are believed to give good efficiency toward corrosion prevention of MS because of the presence of polar groups in their molecular structure and they have tendency to form a complex with the metal surface, both of these features make possible to strengthen the adsorption process on the metal surfaces in aggressive solution.

Three isoxazoline compounds were synthesized in our laboratory and they are characterized using Fourier transform infrared (FTIR) and ^{1}H nuclear magnetic resonance (NMR) spectroscopy techniques. The effectiveness of the synthesized isoxazoline derivatives has been assessed as corrosion inhibitors for MS in 1M H_2SO_4 by electrochemical and non-electrochemical techniques. The morphology of MS with the isoxazoline derivatives has been verified by scanning electron microscope (SEM) and atomic force microscopy (AFM) techniques. To complement the experimental evidence, density-functional theory has been applied to compute electronic properties possibly relevant to the inhibition action (Ref 14). The experimental data can be correlated well with molecular dynamic (MD) simulations (Ref 15-17).

2. Materials and Methods

2.1 Synthesis of Inhibitors

Isoxazoline derivatives were synthesized in two steps as per the reported procedure (Ref 18). The structure of the investigated compounds was shown below.

FTIR spectra were recorded using IR Affinity 1 spectrometer (Shimadzu) and Bruker model using DMSO (solvent) for NMR have been used for the characterization of the synthesized compounds.

PAMHI Yield: 87%, brown solid, IR Spectrum (ν/cm^{-1}): 3295.52 (NH); 1590.38 (C=N), 1317.44 (>C-O-N<); 3380.40 (OH), 1546.98, 1417.74 >C=C< (Ar). ^{1}H NMR (300 MHz, DMSO solvent-d6) δ (ppm): 5.37 (1H, OH), 4.01 (1H, C-NH), 5.93 (CH methine), 3.84 (3H, -OCH_3), 6.48-7.29 (5H, Ar-H), 6.94-7.23 (4H, Ar-H).

PAMI Yield: 77%, pale brown color solid, IR Spectrum (ν/cm^{-1}): 3294.56 (NH); 1599.06 (C=N), 1306.83 (>C-O-N<); 1529.62, 1472.71 >C=C< (Ar); ^{1}H NMR (300 MHz, DMSO solvent -d6) δ (ppm): 4.0 (1H, C-NH), 5.95 (CH methine), 3.83 (3H, -OCH_3), 6.45-7.25 (5H, Ar-H), 6.95-7.27 (4H, Ar-H).

PAHI Yield: 75%, Gray color solid, IR Spectrum (ν/cm^{-1}): 3325.42 (NH); 1551.80 (C=N), 1369.52 (>C-O-N<); 3449.84 (OH), 1551.80, 1420.63 >C=C< (Ar); ^{1}H NMR (300 MHz, DMSO solvent-d6) δ (ppm): 5.36 (1H, OH), 4.02 (1H, C-NH), 5.95 (CH methine), 6.48-7.21 (5H, Ar-H), 6.68-7.17 (4H, Ar-H).

2.2 Electrode Composition

Composition of MS (in %) is 0.084 - C, 0.369 - Mn, 0.129-Si, 0.025 -P, 0.027 - S, 0.022 - Cr, 0.011 - Mo, 0.013 - Ni and the remaining iron were used for weight loss and electrochemical measurements. MS specimen of size 1cm × 3cm × 0.0 cm and 0.785 cm^2 area was used for the same measurements mentioned above. MS coupons were polished by using emery sheets of different grades (200, 400, 600 and 1200) and solvent (trichloroethylene) for degreasing purpose, then the coupons are dried, then finally kept in a desiccator (absorption of moisture can be avoided).

2.3 Non-Electrochemical and Electrochemical Measurements

ASTM standard G31-72 procedure was followed to carry out gravimetric corrosion measurements. Inhibition efficiency (IE %), corrosion rate (CR) and surface coverage (θ) were calculated by the formulae used in the literatures (Ref 4).

The electrochemical measurements were recorded using computer-controlled potentiostat (IVIUM Compactstat Potentiostat/Galvanostat). MS specimens were immersed, half an hour for stabilization period was observed for E_{ocp} prior to the impedance measurements in order to get stable value. Corrosion potentials over a frequency range of 10-0.01 Hz, 10 mV as signal amplitude was set to measure the impedance parameters. Real part (Z′) as well as imaginary part (Z″) were measured at various frequencies. The parameters such as charge transfer resistance (R_{ct}) and double layer capacitance (C_{dl}) were calculated from a plot of Z′ Vs Z″. In the same cell, after EIS studies, potential range of -200 mV to +200 mV with respect to open circuit potential at a sweep rate of 0.5 mV/sec were set for polarization measurements and the electrochemical parameters and inhibition efficiency were determined from the plot.

2.4 Surface Examination Study

SEM and AFM studies were carried out to observe the changes in the MS surface with and without inhibitors. At 303 K, MS specimens were dipped into the corrosive solution containing with and without optimal concentration of the inhibitors for 6 hours using the equipment NTMDT, NTEGRA prima.

2.5 Computational Details

Quantum chemical computations were used to sketch the inhibitors' molecular structures. DFT (density-functional theory) using (B3LYP) with 6-311G (d,p) basis set implemented in Gaussian09 software package was used to accomplish complete geometrical optimization of the examined molecules (Ref 19-25). This method has been demonstrated to produce advantageous geometries for a wide range of systems. Because electrochemical corrosion occurs in the liquid phase, the impact of the solvent must be included into the calculations. The molecular properties obtained, such as the energy of the highest occupied molecular orbital (E_{HOMO}), the energy of the lowest unoccupied molecular orbital (E_{LUMO}), the energy gap (ΔE), electronegativity (χ), global hardness (η), global electrophilicity index (ω) and total energy (TE), were then used to elucidate the reactive sites in the various structures and the reactivity trends among structures. In addition, the experimental data were compared to the trends in the computed quantum chemical descriptors.

The study of the behavior of reactivity between the active sites of the selected isoxazolines and the iron atoms (110) of the metal surface was carried out by molecular dynamics (MD) simulation (Ref 26). This simulation was carried out taking into account the experimental conditions. For this purpose and utilizing Material studio software (Ref 27). We have built a crystalline system that carries six layers of iron atoms emptied by a distance of 19.9 Å with a supercell of size 27.30* 27.30* 37.13 $Å^3$ and with a supercell range (11 x 11). This vacuum contains $5H_3O^+$, $5Cl^-$, 500 H_2O and an only one monomer optimized for each simulation. Before starting the simulation, the compass was utilized as a force field, the dynamics run parameter are Ensemble NVT at 303 et 333 K, simulation time 400 ps with time step 1 fs, spline width 1 Å, cutoff distance 15.5 Å, buffer width 0.5 Å and Thermostat Andersen (Ref [28, 29]).

The interaction ($E_{interaction}$) and binding ($E_{binding}$) energies of our system were defined as follows, respectively (Ref 30):

$$E_{\text{interaction}} = E_{\text{total}} - (E_{\text{surface+solution}} + E_{\text{inhibitor}}) \quad \text{(Eq 1)}$$

$$E_{\text{binding}} = E_{\text{interaction}} \quad \text{(Eq 2)}$$

Where E_{total} translates total energy of our system.

3. Results and Discussion

3.1 Non-Electrochemical Method - Weight Loss Method

Various concentrations (0.5-10 mM) of the isoxazolines synthesized for this study were tested in 1 M H_2SO_4 for a period of 3 hours. The values in Table 1 indicates that by increasing the concentration of isoxazoline concentrations, weight loss as well as corrosion rate of MS were found to decrease which tends to increase the percentage inhibition efficiency (η_{WL} %). This trend could result from the adsorption of isoxazoline molecules and also the area of surface coverage rises with an increase in the inhibitor concentrations that is owing to the formation of stable film on the MS surface (Ref 31-35). At highest concentrations of isoxazolines say 10 mM, more than 90% inhibition efficiency was achieved which confirmed that synthesized isoxazolines were agreed to be potential inhibitors for the prevention of MS. This happened due to the presence of active sites in the isoxazoline derivatives like –NH group, π-bonds in benzene group and N, O atoms where the lone pair of electrons are present on those atoms (Ref 36-39). According to their inhibition efficiencies, the ranking order of the isoxazoline derivatives follows the sequence order: PAMHI > PAMI > PAHI.

3.2 Electrochemical Measurements

3.2.1 Electrochemical Impedance Spectroscopy (EIS). Impedance parameters like charge transfer resistance (R_p), double layer capacitance (C_{dl}) and inhibition efficiency are presented in Table 2 for the absence and the presence of various concentrations of isoxazolines (PAMHI, PAMI and PAHI) in 1 M H_2SO_4 and the impedance curves are depicted in Fig. 1. From both figure and table, it is revealed that when the inhibitors (PAMHI, PAMI and PAHI) concentration increases, there is an increase in diameter of the semicircle and then the impedance spectra displayed one single depressed semicircle which suggested that MS corrosion is controlled by the charge transfer process and furthermore addition of isoxazoline inhibitors did not change any mechanism of MS dissolution (Ref 40). The polarization resistance is measured by the difference in real impedance at lower and higher frequencies. When the concentrations of the isoxazoline inhibitors increases, its electrical capacity decreases may be revealed that protective layer might get formed on the electrode surface (Ref 41). The equivalent circuit (Fig. 1) is used to match the impedance spectra and extract various characteristics like electrolyte resistance (R_e), charge transfer resistance (R_{ct}), inhibitor film resistance (R_f) and polarization resistance (R_P).

The R_P denotes the sum between R_f and R_{ct}. As a result of the electrode surface heterogeneity, constant phase elements

Table 1 Mass loss, Corrosion rate, inhibition efficiency and surface coverage (θ) of mild steel immersed in 1 M H_2SO_4 at various concentrations of PAMHI, PAMI and PAHI at 303 K

Name of the inhibitor	Inhibitor con., mM	Mass Loss, g	Inhibition efficiency, %	Corrosion rate, g cm^{-2} h^{-1}	Surface coverage, θ
Blank	…	0.2059	…	13.34	…
PAMHI	0.5	0.0389	81.1	2.52	0.811
	2.5	0.0204	90.1	1.32	0.901
	5.0	0.0153	92.6	0.99	0.926
	7.5	0.0142	93.1	0.92	0.931
	10.0	0.0094	95.9	0.80	0.959
PAMI	0.5	0.0890	56.8	5.77	0.568
	2.5	0.0526	74.5	3.41	0.745
	5.0	0.0370	82.0	2.40	0.820
	7.5	0.0218	89.4	1.41	0.894
	10.0	0.0119	94.2	0.77	0.942
PAHI	0.5	0.1087	47.2	7.04	0.472
	2.5	0.0318	84.6	2.06	0.846
	5.0	0.0279	86.4	1.81	0.864
	7.5	0.0164	92.0	1.06	0.920
	10.0	0.0139	93.2	0.90	0.932

Table 2 EIS data for MS in 1 M H_2SO_4 electrolyte alone and with PAMHI, PAMI and PAHI.

				CPE					
Medium	Conc., mM	R_e, Ω cm^2	R_p, Ω cm^2	Q×10^5, μF s^{n-1} cm^{-2}	n	C_{dl}, μF cm^{-2}	τ, mS	χ×10^{-4}	η_Z, %
Blank	—	1.06±0.02	011.03±0.05	11.71±0.11	0.823±0.007	28.2	0.311	0.8	—
PAMHI	0.5	1.78±0.05	061.80±0.08	07.94±0.05	0.827±0.006	24.8	1.532	0.3	82.2
	2.5	5.33±0.04	106.70±0.07	02.25±0.09	0.826±0.006	22.5	2.400	0.6	89.7
PAMI	5.0	1.72±0.04	125.54±0.13	05.86±0.11	0.832±0.006	21.0	2.549	0.7	91.2
	7.5	1.44±0.02	163.60±1.23	04.77±0.09	0.843±0.002	19.3	3.157	2.1	93.3
	10	7.63±0.08	237.50±2.50	02.20±0.02	0.847±0.004	17.5	4.156	1.7	95.3
	0.5	1.62±0.07	024.50±0.22	08.32±0.13	0.838±0.004	25.1	0.615	0.9	55.0
	2.5	1.51±0.05	041.00±0.16	07.32±0.11	0.839±0.002	24.0	0.984	1.1	73.1
	5.0	1.66±0.03	056.80±0.45	06.80±0.15	0.840±0.001	23.6	1.340	0.7	80.6
	7.5	1.33±0.06	113.71±0.35	05.23±0.09	0.847±0.005	22.1	2.513	1.5	90.3
	10	1.58±0.06	150.10±1.54	05.07±0.04	0.851±0.007	21.6	3.242	80.61.1	92.6
PAHI	0.5	1.88±0.06	021.38±0.23	09.48±0.13	0.829±0.004	26.4	0.564	1.5	48.4
	2.5	1.13±0.03	068.51±0.41	07.26±0.24	0.831±0.002	24.7	1.692	0.9	83.9
	5.0	1.61±0.02	094.60±0.78	06.53±0.10	0.835±0.004	23.9	2.260	1.7	88.3
	7.5	1.44±0.07	101.19±0.54	06.07±0.19	0.838±0.003	22.7	2.297	0.8	89.1
	10	1.87±0.04	112.55±1.20	05.57±0.08	0.844±0.005	21.8	2.453	1.4	90.2

(CPE) are employed in place of double layer capacitance (C_{dl}) (Ref 42). The physical expression of CPE impedance is (Ref 42):

$$Z_{\mathrm{CPE}} = \frac{1}{Q^1 \times (i \times \omega)^n} \quad \text{(Eq 5)}$$

Where Q, i, ω and n stand for CPE constant, imaginary number, angular frequency and phase shift, respectively. n symbolizes the deviation from the ideal behavior ranging from 0 and 1. Equation. (6) defines the relationship between the impedance of the CPE and the C_{dl} (Ref 43):

$$C_{\mathrm{dl}} = \left(Q^{1/n}(R_P)^{1-n/n}\right) \quad \text{(Eq 6)}$$

with (τ), the charge transfer process's time constant is computed as:

$$t = C_{\mathrm{dl}} R_p \quad \text{(Eq 7)}$$

Chi-square element was surveyed to verify the accuracy of the fitted data. All the outcomes provided a less (10^{-3}) values of Chi-square (Table 2), mirroring the good agreement between the fitting information and the experimental finding. The inhibiting performance (η_Z) generated by EIS is given by the next expression:

$$\eta_Z(\%) = \left(1 - \frac{R_p^0}{R_p}\right) \times 100 \quad \text{(Eq 8)}$$

where R_p^0 and R_p corresponding to the polarization resistances in the uninhibited and inhibited electrolyte, respectively.

When there is an increase in isoxazoline inhibitor concentration, the thickness of the protective layer increases because more PAMHI, PAMI and PAHI would be adsorbed on the electrode surface electrostatically, which results in an observable decrease in C_{dl}. This tendency is in accordance with

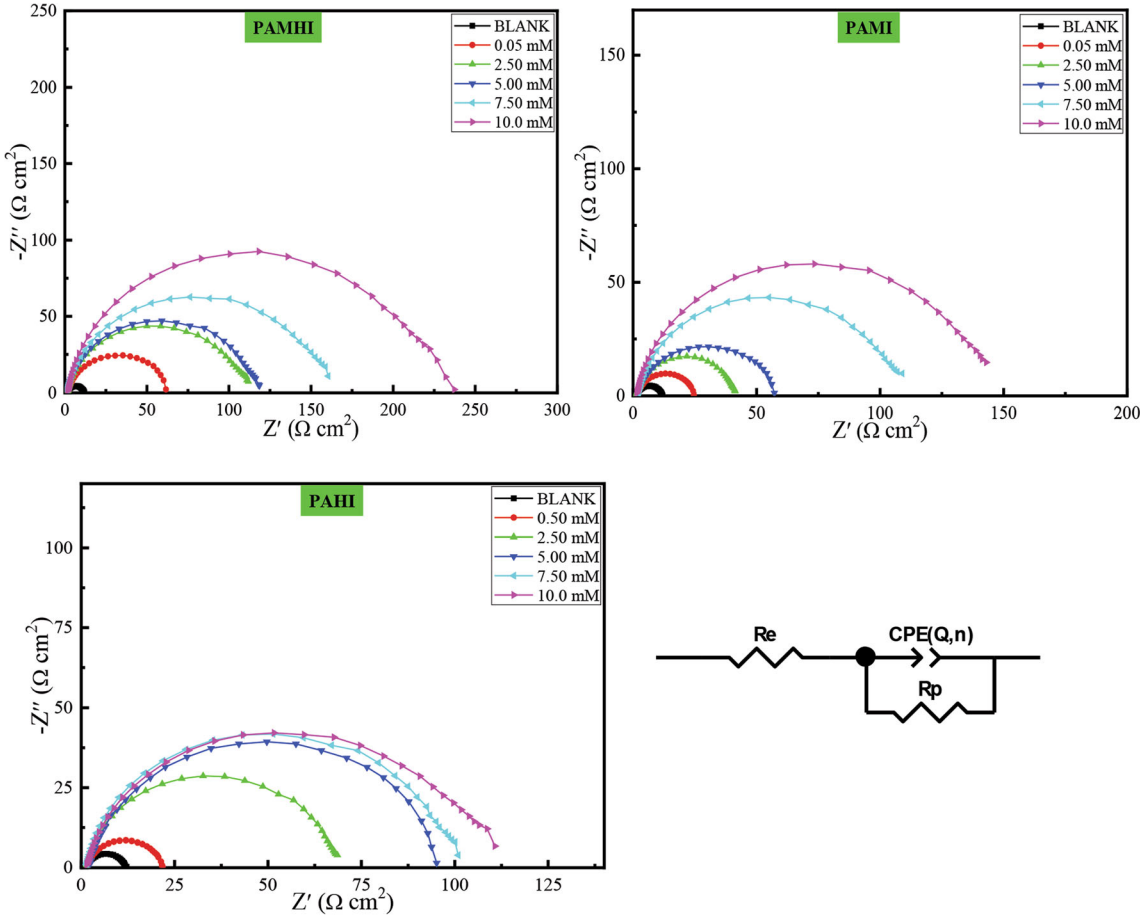

Fig. 1. Nyquist diagram for mild steel in 1 M H_2SO_4 for selected concentrations of inhibitors: PAMHI, PAMI and PAHI and the employed circuit for fitting EIS spectra

Helmholtz model. A barrier was created by the inhibitor film between MS surface and aggressive solution (Ref 44) for the studied inhibitors where the inhibition efficiency was increased due to the protective film formation on the MS surface. The uncontrolled electrolyte had higher Q values than the inhibited electrolyte, indicating that the studied molecules interacted with the MS surface, inhibiting the metal's exposed active sites. Indeed, the uninhibited system's n value is smaller than that of the system with PAMHI, PAMI and PAHI, indicating a decrease in surface heterogeneity (Ref 45). Values of inhibitive performance η_Z rise with the amount of PAMHI, PAMI and PAHI up to 93.3% for PAMHI, 92.6% for PAMI and 89.6% for PAHI at 10 mM. It is worth mentioning that the value of the relaxation time constant (s) slowly increases with isoxazoline derivatives concentration as well and the time of adsorption process becomes therefore much higher which means a slow adsorption process (Ref 46, 47). PAMHI has the highest value of s, implying that PAMHI was the slowest in the adsorption processes.

3.3 Potentiodynamic Polarization Measurements

Electrochemical parameters such as i_{corr}, E_{corr}, b_a and b_c values obtained from Tafel plots extracted from these curves are shown in Table 3 for MS in 1 M H_2SO_4 containing various concentrations of isoxazolines as shown in Fig. 2. The obtained i_{corr} values were decreased with increase in inhibitor concentration and percentage η_P increased as well. After the addition of isoxazoline compounds to the acid solution, anodic metal dissolution of iron and cathodic reactions were inhibited and this trend can be seen from Fig. 2.

The results revealed that the adsorption takes place on the active sites of MS surface by the isoxazoline inhibitor molecules (Ref 48). Moreover, when the isoxazoline concentration increases, both anodic and cathodic reactions are more pronounced which indicates that the cathodic Tafel slopes (b_c) of isoxazolines derivatives changed with inhibitor concentration which denote that inhibitors controlled by cathodic reactions. However, the anodic polarization plot is less pronounced compared to that of the cathodic polarization plot. The addition of isoxazolines to the aggressive solution does not modify the reduction mechanism because the parallel lines were obtained by the cathodic current potential curves and the reduction takes place mainly through a charge transfer mechanism at MS surface (Ref 49-51). These results suggested that the presence of isoxazolines (PAMHI and PAHI) inhibited iron oxidation and in a lower extent undergoes cathodic reduction reaction. Further inspection of the isoxazoline (PAMI) revealed that on increasing the concentration both anodic and cathodic current densities were shifted. Hence, it can be concluded that PAMI behaved as mixed type, since electrode potential displacement is lower than 85 mV in any direction. However, in inhibitors (PAMHI and PAHI) minor shift of E_{corr} values toward negative direction suggests the predominant cathodic control over the reaction.

Table 3 The extracted parameters from Tafel plots for the MS/1 M H_2SO_4 system in the presence and absence of PAMHI, PAMI and PAHI at 303 K

Medium	Conc, mM	$-b_c$, mV dec^{-1}	$-E_{corr}$, mV/SCE	i_{corr}, μA cm^{-2}	η_p, %
Blank	…	97	460.1	785.0	…
PAMHI	0.5	133	469.7	143.2	81.8
	2.5	116	457.7	101.3	87.1
	5.0	113	446.9	093.1	88.1
	7.5	101	473.6	47.46	93.9
	10	111	455.3	042.5	94.6
PAMI	0.5	153	491.4	360.0	54.1
	2.5	124	458.3	199.6	74.6
	5.0	147	476.4	141.9	81.9
	7.5	231	435.1	86.11	89.0
	10	145	440.7	070.6	91.0
PAHI	0.5	148	476.3	403.7	48.6
	2.5	163	452.3	112.8	85.6
	5.0	232	437.1	085.7	89.1
	7.5	123	514.2	078.9	89.9
	10	155	430.7	071.8	91.0

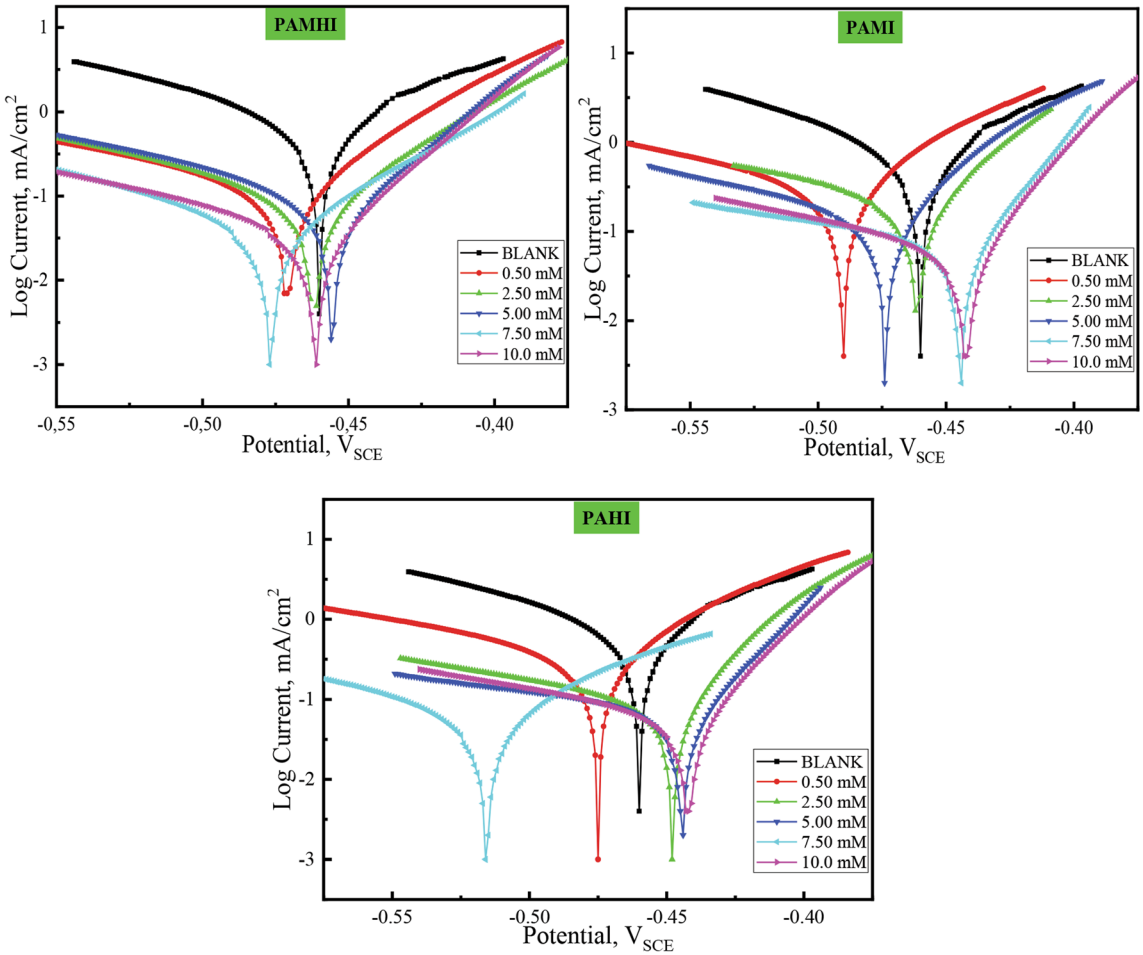

Fig. 2. Tafel plots for the MS/ 1 M H_2SO_4 system in the presence and absence of various amounts of PAMHI, PAMI and PAHI at 303 K

The inhibiting performance (η_p) comes from polarization measurement is determined by the following equation:

$$\eta_p(\%) = \left(1 - \frac{i_{cr}}{i^0_{cr}}\right) \times 100 \qquad \text{(Eq 9)}$$

where i^0_{cr} and i_{cr} corresponding to the corrosion current densities values in the uninhibited and inhibited electrolyte, respectively.

3.4 Adsorption Isotherm

How the interaction between the studied isoxazoline molecules as inhibitors and metal surface (MS) can be studied? The answer is it can be studied by the adsorption isotherm which provides basic and important information (Ref 52, 53). To obtain an isotherm, it is necessary to find the linear relation between θ values and C. Based on the experimental findings, Langmuir adsorption was obeyed by the inhibitor and it was plotted by considering one of the most accurate studies, viz., polarization measurements. According to Langmuir's assumptions, all the adsorption sites are comparable and the binding of the particle takes place independently from nearby sites whether occupied or not.

According to this isotherm, the following equation relates θ and C

$$\frac{C}{\theta} = \frac{1}{K_{ads}} + C \qquad \text{(Eq 3)}$$

Intercept values were calculated from the plot of C/θ-axis (Fig. 3) and calculated K_{ads} values can be related to free energy of adsorption, ΔG°_{ads} as given by

$$K_{\text{ads}} = \frac{1}{C_{H_2O}} \times e^{\frac{-\Delta G^{0}_{\text{ads}}}{RT}} \qquad \text{(Eq 4)}$$

where R is the universal gas constant, T is the temperature, which equal to 303 K and is the concentration of water in solution, which equal to 55.5 mol L^{-1}.

The validity of this approach was confirmed with the regression coefficients values (R^2= 0.9982). A straight line was obtained when a graph was plotted C/θ versus C (Fig. 3) where slope value is close to unity which indicates that adsorption of isoxazolines comply with Langmuir's adsorption isotherm which also implies that adsorbed inhibitor molecules form monolayer on the surface of MS and there is no interaction among the adsorbed inhibitor molecules (Ref 54). In case of isoxazoline molecules, the calculated ΔG°_{ads} values were found between −28.52 and −33.44 kJ mol^{-1} which confirmed the mixed type of adsorption (Table 4).

3.5 Surface Characterization

The surface morphologies of MS after being exposed to the acid solution with and without inhibitors are presented in Fig. 4 and 5 for SEM and AFM, respectively.

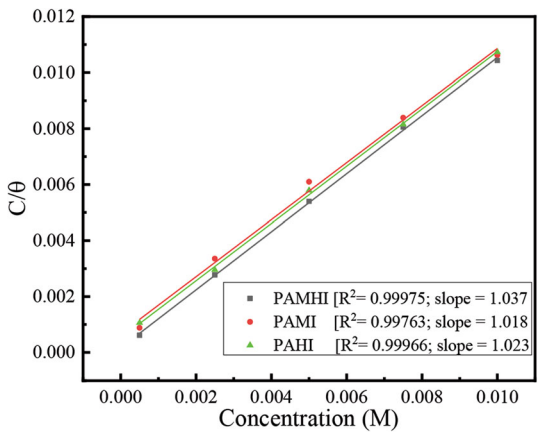

Fig. 3. Langmuir plot of inhibitors in 1 M H_2SO_4

As far as SEM is considered, the surface of MS without inhibitor in acid solution is extremely spoiled with clear cracks, whereas for the inhibited MS is smooth with some white stripes, which may be the protective film. The predominant difference of appearance between the exposed and unexposed MS surface implies that the adsorption of active isoxazolines on the MS surface prevents the metal from the corrosion attack. In relation to the AFM method, it is being used mainly for measuring the three dimensional topography (Ref 55). It is known from the images that the surface of the specimen immersed in 1 M H_2SO_4 presented more roughness of 145.71 nm whereas MS immersed in the acid solution containing PAMHI whose roughness was 26.37 nm. The decreased roughness value in the presence of PAMHI confirmed the formation of protective layer on the MS surface.

3.6 Quantum Chemical Studies

3.6.1 Neutral Form of the Studied Inhibitors. Relation between the molecular structures of the inhibitors and their inhibitive effects toward acid corrosion can be studied through quantum chemical calculations (Ref 56, 57). In addition, DFT is also used to study the physical characteristics of the inhibitor/surface process (Ref 58-60). In non-protonated form of the isoxazoline derivatives, optimized structures, HOMOs and LUMOs in aqueous phase have been depicted in Table 5. It became clear that the HOMO electron density distribution occupies the majority of the surface skeleton of the selected molecules. This result indicates that the acceptability of electrons from the iron surface is very high, in this case, there are several active local electrons accepted sites distributed throughout the structure of the molecules studied. While the HOMO electron density distribution is localized over most of the surface of the molecules studied except for the substitutional grouping of PAMI and PAHI molecules. In addition, the attached substitutional group of the PAMHI molecule carries a lower proportion of the HOMO density is possibly due to OH and OCH_3 substituents. This observation justified the inhibitory performance of this molecule.

The main quantum chemical descriptors for the inhibitors PAMHI, PAMI and PAHI were tabulated in Table 6. Based on the calculated values of the E_{HOMO} and ΔN descriptors of the three compounds, it is well known that PAMHI molecule has high values of these descriptors, reflecting a high electron donating power of the vacant orbitals of the iron atoms located on the surface of the metal (Ref 61). This result confirmed the high value of the inhibitory efficiency obtained by this molecule. Thus, the very close values of E_{HOMO} and ΔN between the two molecules PAHI and PAMI show that the two electron donor groups by OH and OCH_3 mesomeric effect behave in the same way.

E_{LUMO} is a very interesting molecular property that identifies the electrophilic capacity of the inhibitory molecule (Ref 62). This characteristic would be able to form π-back bonds by receiving electrons from the metal via the π* orbitals (Ref 63). The low E_{LUMO} values of the molecules studied reflects high capability to receive electrons from the metal surface. Gap energy (ΔE_{gap}), dipole moment (μ), global hardness (η) and total energy (TE) are critical factors defining the reactivity of the molecule. Since the values of ΔE, η and TE are low and the μ value is high, the inhibitory molecule is more reactive (Ref 64). The values of these three descriptors of three studied molecules are joined together in Table 6, it is well noted

Table 4 Adsorption parameters of PAMHI, PAMI and PAHI for MS in 1M H_2SO_4 electrolyte

Name of the inhibitor	Slope	Linear regression coefficient, R^2	K_{ads}, L mol^{-1}	ΔG°_{ads}, kJ mol^{-1}
PAMHI	1.037	0.99975	6031.69	−32.05
PAMI	1.018	0.99763	1485.08	−28.52
PAHI	1.023	0.99966	1918.45	−33.44

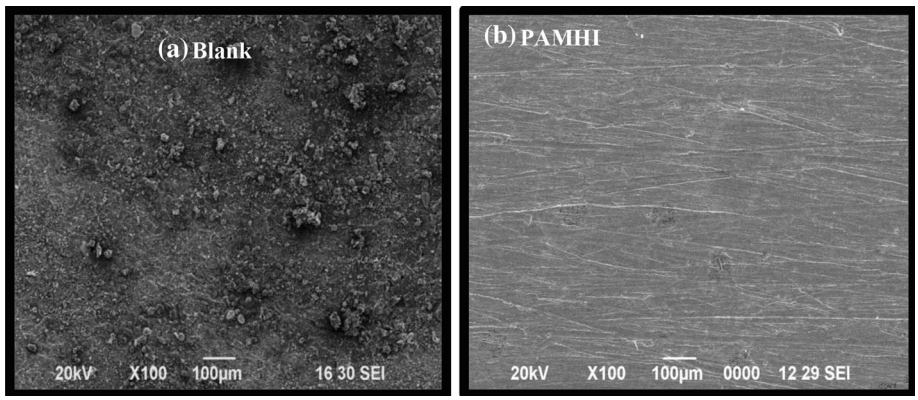

Fig. 4. SEM images for (a) MS recorded in 1 M H_2SO_4 (b) MS recorded in 1 M H_2SO_4 for with inhibitor (PAMHI)

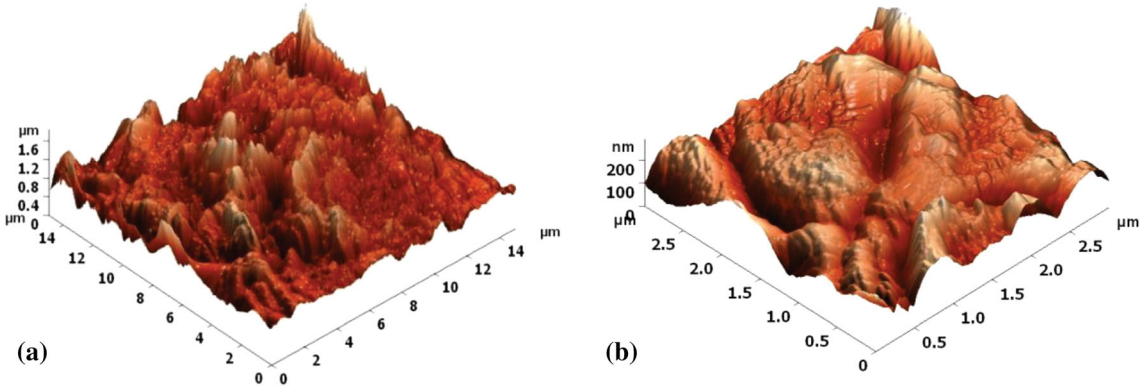

Fig. 5. AFM micrographs for mild steel in 1 M H_2SO_4 in (a) absence of inhibitor (Blank) (b) presence of inhibitors (PAMHI)

that the PAHMI molecule satisfies the preceding criteria, which affirms its larger capacity to inhibit the corrosion of metal. The calculations results obtained from the neutral inhibitor molecules in the aqueous phase confirm the order of the inhibitory efficiency of these inhibitors.

3.6.2 Protonated Form of the Studied Inhibitors. The optimized structures, HOMOs and LUMOs of the isoxazolines derivatives in protonated form in aqueous phase are given in Table 7.

The nitrogen atom N9 is considered to be the most available site for fixing the proton H^+. It is evident that the HOMO and LUMO electron density distribution has changed very remarkably compared to the neutral forms of the molecules under investigation. The quantum chemical descriptors values are grouped in Table 8. It seems very interesting to view that the majority of the values of these descriptors are in agreement with the order of inhibitory efficiency of the molecule tested (PAMHI > PAMI > PAHI). In acid medium, the obtained results revealed that the protonated form of the inhibitors should make a higher contribution to the corrosion inhibiting effect of the isoxazolines on the metal surface (Ref 65).

3.6.3 Mulliken Charge Density Distribution. Tables 9 and 10 show the values of Mulliken charge distributions for non-protonated and protonated forms. It has been reported in the literature that if the atomic charges of adsorbed atoms present in the molecules are more negative, then the atom can easily donate its electrons to the unoccupied orbital of the metal atoms (Ref 66-68).

In non-protonated form, higher charge densities are observed for O and N atoms which are the regions of the highest electron density and electrophiles can attack easily. N atoms have negative charge so they are the active centers and have the ability of bonding to the metal surface is too strong. In protonated form, O and some of the carbon atoms in the isoxazolines have negative charges which are capable of bonding to the metal surface. Conversely, nitrogen and some carbon atoms carry positive charges, which are the active sites to nucleophiles for the attack. These factors will add strength to

Table 5 Optimized structures and FMO electron density distribution for the neutral forms of PAMHI, PAMI and PAHI at B3LYP/6-311G (d, p) in aqueous phase

Inhibitors	Optimized structures	HOMOs	LUMOs
PAMHI	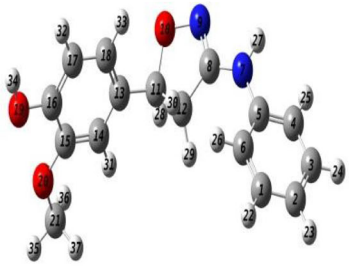	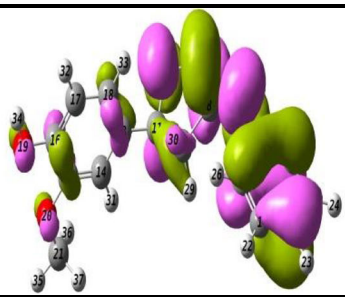	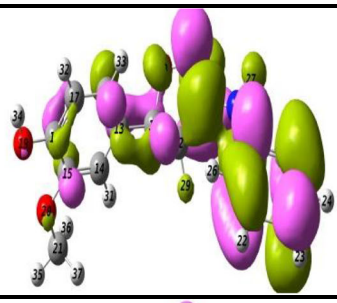
PAMI	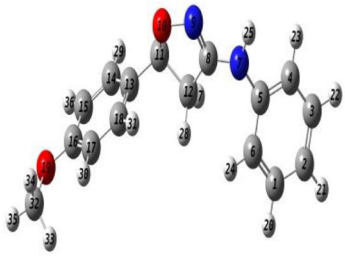	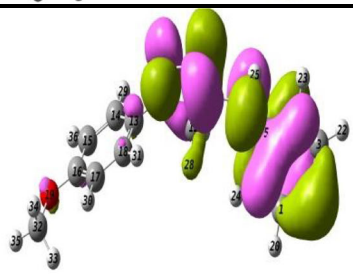	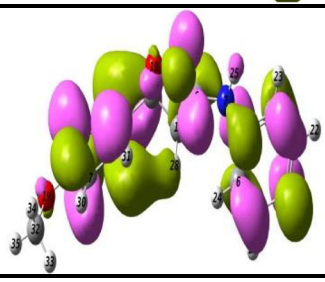
PAHI	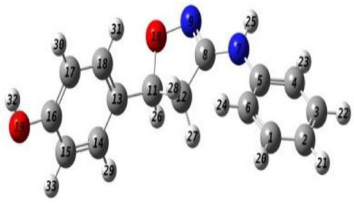	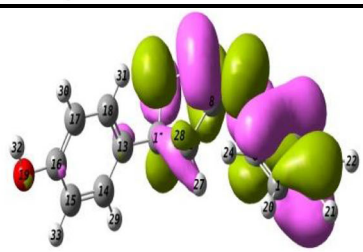	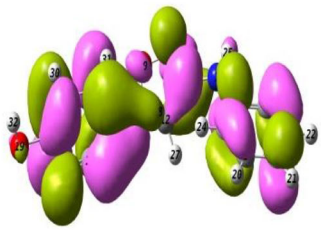

Table 6 Calculated quantum chemical parameters for the inhibitors in non-protonated form obtained utilizing DFT at the B3LYP/6-311G(d,p) basis set in aqueous phase

Quantum chemical descriptors	PAMHI	PAMI	PAHI
Total energy (a u)	−954.48	−879.453	−840.145
μ (D)	4.583	4.545	4.4768
E_{HOMO} (eV)	−5.385	−5.627	−5.627
E_{LUMO} (eV)	−0.315	−0.548	−0.545
ΔE_{gap} (eV)	5.069	5.079	5.082
IP (eV)	5.385	5.627	5.627
EA (eV)	0.3153	0.548	0.545
η (eV)	2.534	2.539	2.541
χ (eV)	2.850	3.087	3.086
ΔN_{110}	0.389	0.341	0.341

the adsorption of the isoxazolines on the MS surface leading to a stable protective layer and thus impeding the further metal corrosion in sulfuric acid solution.

3.6.4 Molecular Dynamic (MD) Simulation. This method is based on the intermolecular interactions between the most relevant atoms and the atoms of the first iron layer (Ref 67). Figure 6 shows the most stable configurations of the inhibitor system and temperature influence.

It is very remarkable that the three compounds adsorb in the same way in which the 4-(3-(phenylamino)-4,5-dihydroisoxazol-5-yl skeleton is the most active part that adsorbs in parallel with the metal surface. While phenyl substituted by either the methoxy group (PAMI) or the hydroxy group (PAHI) or both (PAMHI) are positioned inclined with respect to the metal surface, therefore, this motive does not participate in the protection of iron steel. In addition, the introduction of

Table 7 Optimized structures and FMO electron density distribution for the protonated forms of PAMHI, PAMI and PAHI at B3LYP/6-311G (d, p) in aqueous phase

Inhibitors	Optimized structures	HOMOs	LUMOs
PAMHI	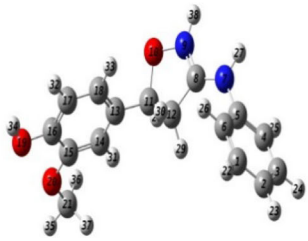	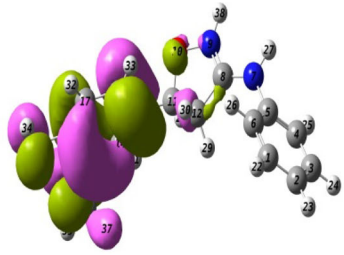	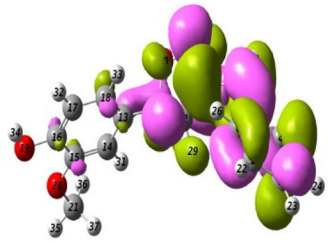
PAMI		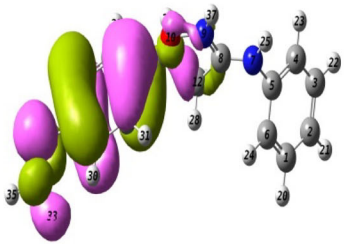	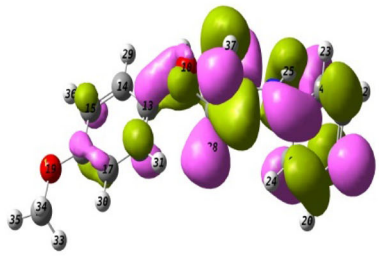
PAHI	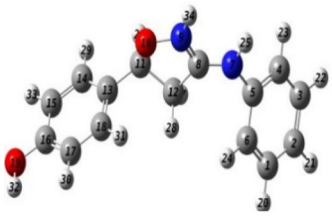	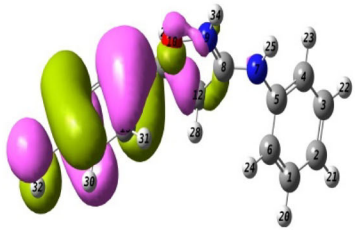	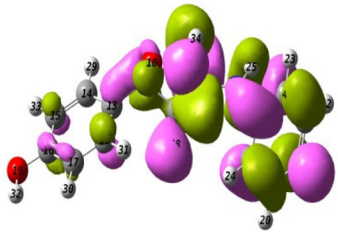

Table 8 Quantum chemical descriptors for the neutral and protonated forms of PAMHI, PAMI and PAHI at B3LYP/6-31G (d, p) in aqueous phase

Quantum chemical descriptors	PAMHI	PAMI	PAHI
Total energy (a u)	−955.137	−879.895	−840.586
μ (D)	11.991	9.707	8.639
E_{HOMO} (eV)	−6.122	−6.525	−6.614
E_{LUMO} (eV)	−1.602	−1.593	−1.633
ΔE_{gap} (eV)	4.52	4.932	4.981
IP (eV)	6.122	6.525	6.614
EA (eV)	1.602	1.593	1.633
η (eV)	2.26	2.466	2.490
χ (eV)	3.862	4.059	4.123
ΔN_{110}	0.212	0.154	0.140

Table 9 Condensed Fukui functions of non-protonated forms PAMHI, PAMI and PAHI in aqueous phase

PAMHI		PAMI		PAHI	
Atoms	Charges	Atoms	Charges	Atoms	Charges
C1	−0.007478	C1	−0.004190	C1	−0.004282
C2	−0.003980	C2	−0.003124	C2	−0.002915
C3	0.002428	C3	0.000178	C3	0.000170
C4	−0.030086	C4	0.009100	C4	0.009086
C5	0.299392	C5	0.152648	C5	0.151860
C6	−0.005369	C6	0.024302	C6	0.024604
N7	−0.366965	N7	−0.222614	N7	−0.222423
C8	0.493523	C8	0.281227	C8	0.282233
N9	−0.278627	N9	−0.204322	N9	−0.204301
O10	−0.448621	O10	−0.346661	O10	−0.347158
C11	0.237682	C11	0.227883	C11	0.230582
C12	0.039895	C12	0.096075	C12	0.094426
C13	0.084896	C13	−0.131213	C13	−0.131735
C14	−0.083407	C14	0.029171	C14	0.030805
C15	0.333278	C15	0.000258	C15	0.003630
C16	0.283975	C16	0.175496	C16	0.154206
C17	−0.036140	C17	−0.018798	C17	−0.012990
C18	−0.039490	C18	0.051536	C18	0.051716
O19	−0.232490	O19	−0.365615	O19	−0.107515
O20	−0.537175	C32	0.248661		
C21	0.294758				

Table 10 Condensed Fukui functions of protonated forms PAMHI, PAMI and PAHI in aqueous phase

PAMHI		PAMI		PAHI	
Atoms	**Charges**	**Atoms**	**Charges**	**Atoms**	**Charges**
C1	0.019226	C1	0.011663	C1	0.011610
C2	0.038450	C2	0.029745	C2	0.029894
C3	0.019343	C3	0.015767	C3	0.015782
C4	0.089271	C4	0.044652	C4	0.044647
C5	0.032172	C5	0.146454	C5	0.145715
C6	0.096690	C6	0.055300	C6	0.055585
N7	−0.147787	N7	−0.195067	N7	−0.195014
C8	0.520901	C8	0.492610	C8	0.494099
N9	0.132262	N9	0.175462	N9	0.175528
O10	−0.272192	O10	−0.281026	O10	−0.281794
C11	0.233385	C11	0.264846	C11	0.267568
C12	0.168014	C12	0.180767	C12	0.179167
C13	−0.135484	C13	−0.142771	C13	−0.143241
C14	0.035287	C14	0.049027	C14	0.051340
C15	0.163857	C15	0.012256	C15	0.015715
C16	0.145352	C16	0.181844	C16	0.160592
C17	0.004602	C17	−0.008131	C17	−0.000897
C18	0.063163	C18	0.073619	C18	0.072776
O19	−0.095920	O19	−0.361497	O19	−0.099073
O20	−0.362154	C32	0.254476		
C21	0.251561				

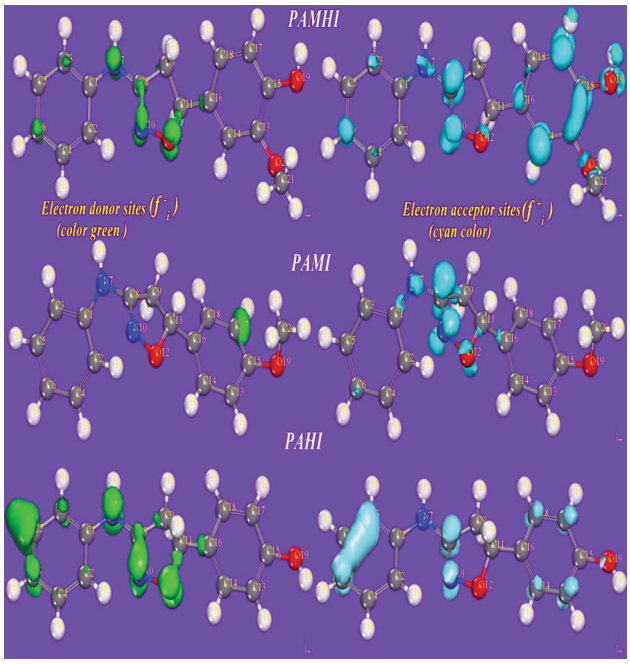

Fig. 6. Active electron donor and acceptor sites of inhibitory molecules using Dmol^3 at the GGA/DNP level

substituents (OH and OCH_3) into the phenyl group is not important. This explains the values closest to the inhibitory efficiencies, for example in the optimal concentration (10 mM) in the experimental part. The temperature increases from 303 to 333 K does not affect the structure of the adsorbed molecules (Fig. 7). Hence, the skeleton of the adsorbed molecules remains unchanged in the two simulated temperatures. The energy values of $E_{interaction}$ and $E_{binding}$ in the two temperatures studied are grouped in Table 11. The comparative analysis of the results obtained shows that the negative values of $E_{interaction}$ reflect a strong interaction between the 4-(3-(phenylamino)-4,5-dihydroisoxazol-5-yl) for the three molecules and the Fe (110) surface atoms (Ref 69).These values are close to each other, reflecting the same interaction behavior of the inhibitors tested.

In addition, high binding energy ($E_{binding}$) values indicate that our inhibitors adsorb more efficiently on the substrate surface (Ref 70). The increase in temperature leads to the increase in the values of $E_{interaction}$ and $E_{binding}$, indicating that temperature influences the interaction and adsorption of skeletal atoms of the inhibitory metal surface, respectively. As a result, the substitution effect has no role in this study.

Temperature is a very important kinetic factor that influences the bonds formed between the inhibitor and the metal surface, this influence has occurred in particular on physical bonds. In this context, we will study the behavior of the interatomic bonds that are established between the hetero atom pairs (N7, N9 and O10) and the iron atoms of the first layer utilizing the RDF function (Ref 71). With the assistance of molecular dynamics simulation, the variation of g (r) vs. r is given in Fig. 8 under the influence of temperature. This figure shows that the RDF for the species studied appeared for the first very noticeable and more intense peak. This indicates the presence of strong interactions between the hetero atoms selected for the three inhibitors (PAMHI, PAMI and PAHI) and iron atoms (Ref 72). This result is demonstrated by the values of interatomic distances (Fe-heteroatom), which are included in the chemisorption interval (1 $\sim$ 3.5 Å) (Ref 73). This indicates that our compounds are effective against corrosion despite the increase in temperature. All these simulation results are in good agreement with those obtained in the experimental part.

3.7 Mechanism of Inhibition and Evaluation of Inhibitors

The inhibitive nature of MS by isoxazolines in 1 M sulfuric acid solution can be studied based on the molecular adsorption theory (Ref 74-76). An adsorption of inhibitor on the metal surface is so fast in acid solution; therefore surface of MS is protected in acid solutions (Ref 77). Inhibition efficiency of the investigated isoxazolines at 10 mM is in the range 93.24-94.22%. The highest inhibition efficiency of the isoxazolines may be due to the presence of aromatic rings, >C=N- groups, -NH and electron donating substituents in the aromatic ring such as OH, OCH_3, which enhances the electron density of the aromatic ring leading to greater adsorption. In acid solution, increasing inhibition efficiency of the isoxazolines follows the order: PAMHI $\cong$ PAMI > PAHI. PAMHI exhibits maximum

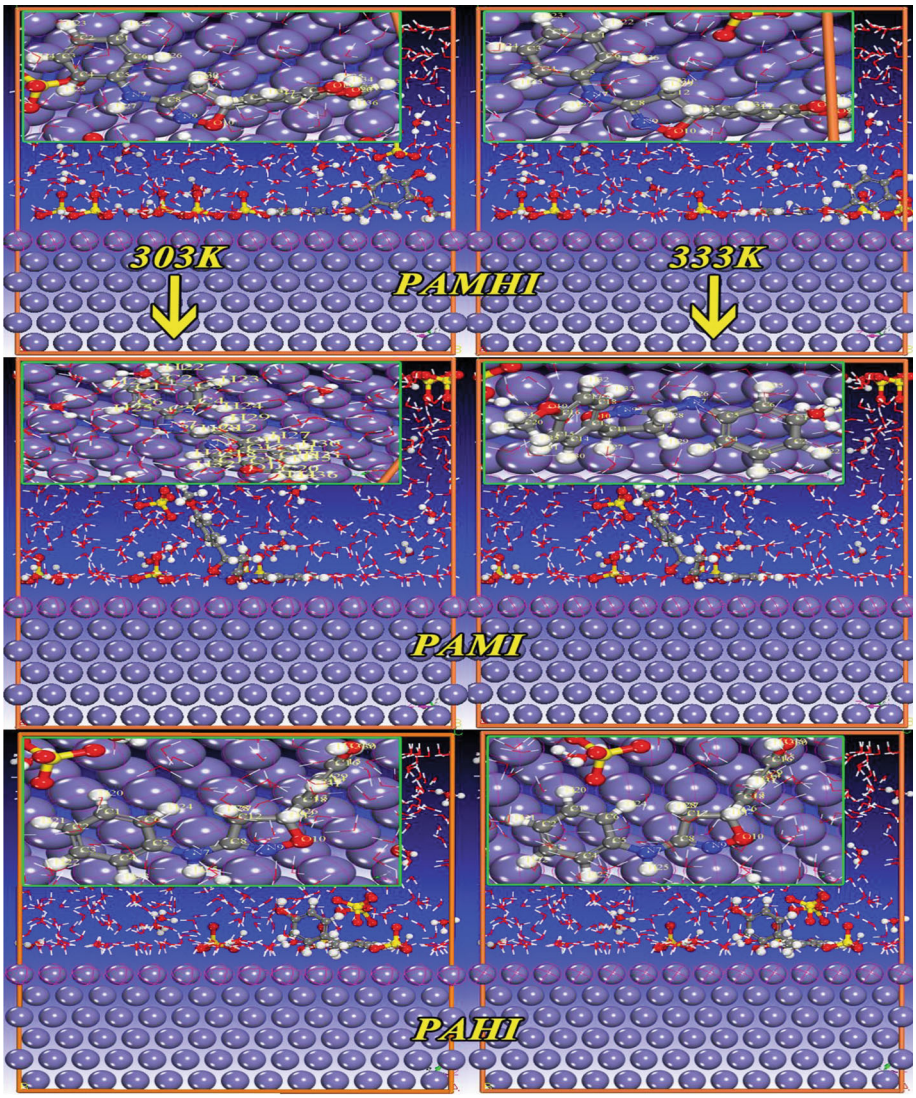

Fig. 7. Stablest configurations of adsorption of isoxazoline derivatives on the Fe (110) surface at 303 and 333 K

Table 11 $E_{interaction}$ **and** $E_{binding}$ **of PAMHI, PAMI and PAHI adsorbed on the iron surface at 303 and 333 K, all in kJ mol^{-1}**

System−inhibitor	303 K		333 K	
	$E_{interaction}$	$E_{binding}$	$E_{interaction}$	$E_{binding}$
System−PAMHI	−227.080	227.080	−209.832	209.832
System−PAMI	−224.741	224.741	−208.011	208.011
System−PAHI	−224.625	224.625	−207.645	207.645

inhibition efficiency (94.46%) due to the presence of electron donating –OCH_3 and –OH groups in the benzene ring attached at fifth position of the isoxazoline ring compared to PAMI and PAHI whereas PAMI shows slightly lower IE 94.22% which is attributed to the presence of only one -OCH_3 group. The inhibitor PAHI shows 93.24% as it contains only one –OH group. The results are in accordance with to the fact that when the number of electron releasing groups increases the electron density on the benzene ring increases, which in turn enhances the %IE (Ref 78-80).

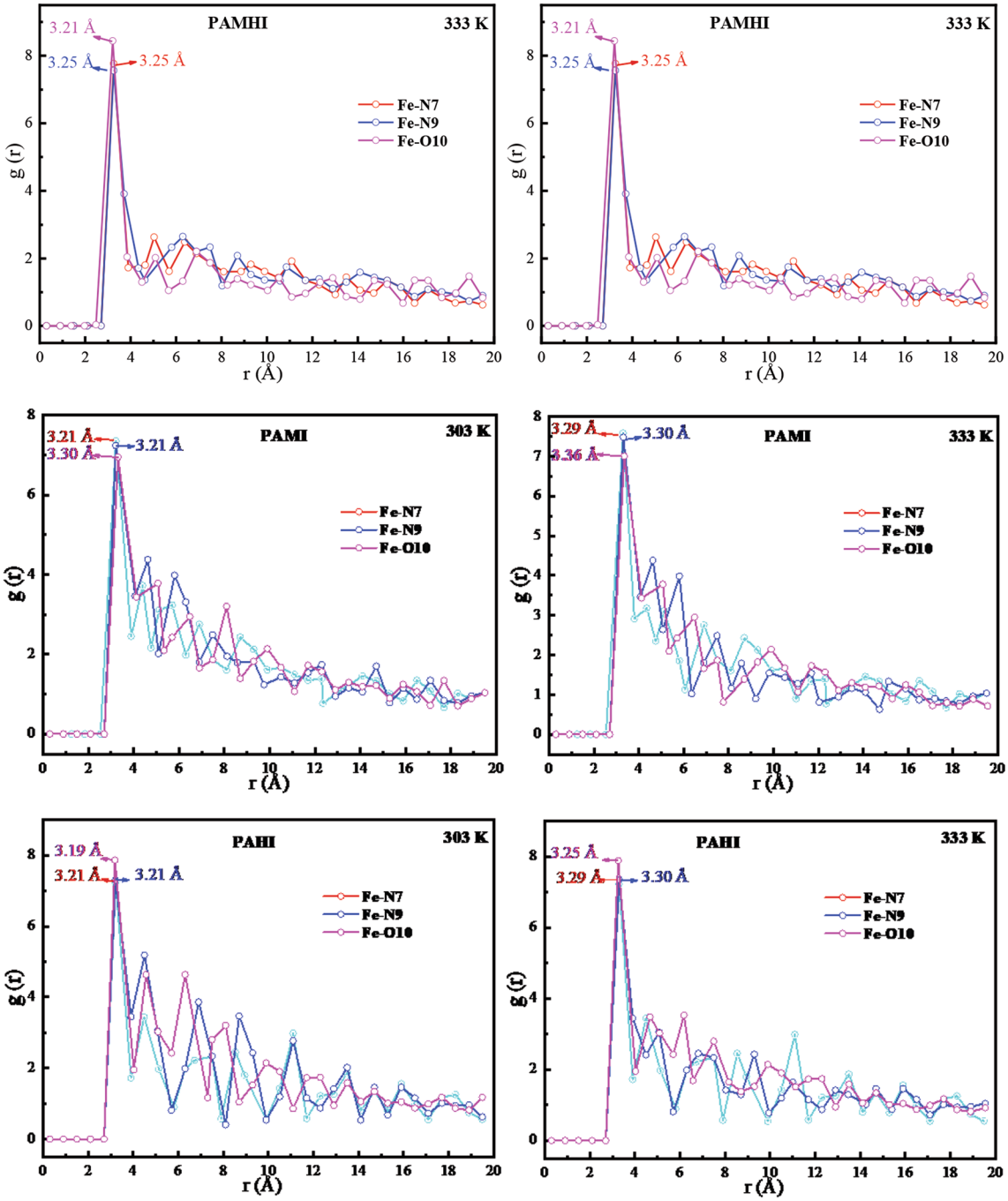

Fig. 8. RDFs of isoxazoline derivatives on Fe (110) surface at 303 and 333 K

4. Conclusions

In this present study, the isoxazoline derivatives were synthesized, characterized and their corrosion inhibition efficiency were evaluated using weight loss, electrochemical, surface and computational studies. The main conclusions were as follows

1. The studied isoxazolines showed very good inhibition performance in 1M H_2SO_4 and examined their inhibition efficiency values which follows the order: PAMHI ≅ PAMI > PAHI at 10 mM concentration.
2. The obtained results proved that the isoxazolines inhibit the corrosion, get adsorbed on the metal surface and followed Langmuir adsorption isotherm. The inhibitors adsorbed through both physical and chemical adsorption processes.
3. Polarization measurements also revealed that the inhibitors are effective and the type of these inhibitors are mixed type.
4. Impedance measurements indicate the charge transfer resistance increase with increasing concentration of the inhibitor.

5. The presence of isoxazoline molecules on the mild steel surface is further supported and confirmed by SEM and AFM analysis.
6. The results obtained from Langmuir adsorption isotherm, SEM and AFM proposed that the mechanism of corrosion inhibition occurs merely through the adsorption method.
7. The results obtained from MD simulation and DFT methods proved that the protonated isoxazoline derivatives were consistent with the experimental results.

Conflict of interest

The authors declare that there are no conflicts of interest regarding the publication of this paper.

References

1. Y. Chen, S. Zheng, J. Zhou, P. Wang, L. Chen and Y. Qi, Influence of H_2S Interaction with Prestrain on the Mechanical Properties of High-Strength X80 Steel, *Int. J. Hydrog. Energy*, 2016, **41**, p 10412–10420.
2. G. Leonzio, Mathematical Modeling and Environmental Analysis of Heat Pumps Integrated in Aprocess to Treat Spent Pickling Liquors, *J. Clean Prod.*, 2016, **133**, p 835–849.
3. M.T. Alhaffar, S.A. Umoren, I.B. Obot and S.A. Ali, Isoxazolidine Derivatives as Corrosion Inhibitors for Low Carbon Steel in HCl Solution: Experimental, Theoretical and Effect of KI Studies, *RSC Adv.*, 2018, **8**, p 1764–1777.
4. V. Saraswat, M. Yadav and I.B. Obot, Investigations on Eco-friendly Corrosion Inhibitors for Mild Steel in Acid Environment: Electrochemical, DFT and Monte Carlo Simulation Approach, *Colloids Surf. A*, 2020, **599**, p 124881.
5. A. Zarrouk, B. Hammouti, A. Dafali and H. Zarrok, L-Cysteine Methyl Ester Hydrochloride: A New Corrosion Inhibitor for Copper in Nitric Acid, *Der Pharma Chem*, 2011, **3**(4), p 266–274.
6. A. Tazouti, M. Galai, R. Touir, M. Ebn Touhami, A. Zarrouk, Y. Ramli, M. Saraçoğlu, S. Kaya, F. Kandemirli and C. Kaya, Experimental and Theoretical Studies for Mild Steel Corrosion Inhibition in 1.0 M HCl by Three New Quinoxalinone Derivatives, *J Mol Liq*, 2016, **221**, p 815–832.
7. Y. ELouadi, F. Abrigach, A. Bouyanzer, R. Touzani, O. Riant, B. ElMahi, A. El Assyry, S. Radi, A. Zarrouk and B. Hammouti, Corrosion Inhibition of Mild Steel by New N-heterocyclic Compound in 1 M HCl: Experimental and Computational Study, *Der Pharma Chem.*, 2015, **7**, p 265–275.
8. H. Zarrok, A. Zarrouk, R. Salghi, H. Oudda, B. Hammouti, M. Ebn Touhami, M. Bouachrine and S. Boukhris, A Combined Experimental and Theoretical Study on the Corrosion Inhibition and Adsorption Behaviour of Quinoxaline Derivative During Carbon Steel Corrosion in Hydrochloric Acid, *Port Electrochim Acta*, 2012, **30**, p 405–417.
9. J. Luo, X. Cheng, C.F. Xinhua Chen, H.X. Zhong, Y.W. Ye, H.C. Zhao, Y. Li and H. Chen, The Effect of N and S Ratios in N, S co-doped Carbon Dot Inhibitor on Metal Protection in 1 M HCl Solution, *J. Taiwan Inst. Chem. Eng.*, 2021, **127**, p 387–398.
10. J. Luo, X. Cheng, C. Zhong, X. Chen, Y.W. Ye, H. Zhao and H. Chen, Effect of Reaction Parameters on the Corrosion Inhibition Behavior of N-doped Carbon Dots for Metal in 1M HCl Solution, *J. Mol. Liq.*, 2021, **338**, p 116783.
11. J. Saranya, K. Lavanya, M. Haritha Kiranmai, R. Subbiah, A. Zarrouk and S. Chitra, Quinoxaline Derivative as Anti-corrosion Additives for Mild Steel, *Corros. Rev.*, 2021 https://doi.org/10.1515/corrrev-2020-0033
12. Brahim El Ibrahimi, Lei Guo (2020) Azole-Based Compounds as Corrosion Inhibitors for Metallic Materials. DOI: https://doi.org/10.5772/intechopen.93040
13. Y. Ye, H.C. DongpingYang, S. Guo, Q. Yang, L. Chen, H. Zhao and L. Wang, A High-efficiency Corrosion Inhibitor of N-doped Citric Acid-Based Carbon Dots for Mild Steel in Hydrochloric Acid Environment, *J. Haz. Mat.*, 2020, **381**, p 121019.
14. M. Parveen, A. Aslam, A. Ahmad, M. Alam, M.R. Silva and P.S.P. Silva, A Facile & Convenient Route for the Stereo Selective Synthesis of Zisoxazol-5(4H)-ones Derivatives Catalysed by Sodium Acetate: Synthesis, Multispectroscopic Properties, Crystal Structure with DFT Calculations, DNA-binding Studies and Molecular Docking Studies, *J. Mol. Struct.*, 2020, **1200**, p 127067.
15. J. Saranya, F. Benhiba, N. Anusuya, R. Subbiah, A. Zarrouk and S. Chitra, Experimental and Computational Approaches on the Pyran Derivatives for Acid Corrosion, *Colloids Surf. A*, 2020, **603**, p 125231.
16. M. Rbaa, F. Benhiba, P. Dohare, L. Lakhrissi, R. Touir, B. Lakhrissi, A. Zarrouk and Y. Lakhrissi, Synthesis of New Epoxy Glucose Derivatives as a Non-toxic Corrosion Inhibitors for Carbon Steel in Molar HCl: Experimental, DFT and MD Simulation, *Chem. Data Collect*, 2020, **27**, p 100394.
17. M. Rbaa, F. Benhiba, M. Galai, S. Abousalem Ashraf, M. Ouakki, C.H. Lai, B. Lakhrissi, C. Jama, I. Warad, M. Ebn Touhami and A. Zarrouk, Synthesis and Characterization of Novel Cu (II) and Zn (II) Complexes of 5- {[(2-Hydroxyethyl) sulfanyl] methyl}-8-Hydroxyquinoline as Effective Acid Corrosion Inhibitor by Experimental and Computational Testings, *Chem. Phys. Lett.*, 2020, **754**, p 137771.
18. M. Farsak, H. Keleş and M. Keleş, A New Corrosion Inhibitor for Protection of Low Carbon Steel in HCl Solution, *Corros. Sci.*, 2015, **98**, p 223–232.
19. A. Zarrouk, B. Hammouti, A. Dafali, M. Bouachrine, H. Zarrok, S. Boukhris and S.S. Al-Deyab, A Theoretical Study on the Inhibition Efficiencies of Some Quinoxalines as Corrosion Inhibitors of Copper in Nitric Acid, *J. Saudi Chem. Soc.*, 2014, **18**, p 450–455.
20. Peralta J, Ogliaro F, Bearpark M, Heyd J, Brothers E, Kudin K, Staroverov V, Kobayashi R, Normand J, Raghavachari K (2013) Gaussian 09, Revision D. 01, Gaussian, Inc.: Wallingford, CT
21. M. El Faydy, F. Benhiba, B. Lakhrissi, M. Ebntouhami, I. Warad, F. Bentiss and A. Zarrouk, The Inhibitive Impact of Both Kinds of 5-isothiocyanatomethyl-8-hydroxyquinoline Derivatives on the Corrosion of Carbon Steel in Acidic Electrolyte, *J. Mol. Liq.*, 2019, **295**, p 111629.
22. R.G. Parr and R.G. Pearson, Absolute Hardness: Companion Parameter to Absolute Electronegativity, *J. Am. Chem. Soc.*, 1983, **105**, p 7512–7516.
23. R. Nabah, F. Benhiba, Y. Ramli, M. Ouakki, M. Cherkaoui, H. Oudda, R. Touir, I. Warad and A. Zarrouk, Corrosion Inhibition Study of 5, 5-diphenylimidazolidine-2, 4-dione for Mild Steel Corrosion in 1 M HCl Solution: Experimental, Theoretical Computational and Monte Carlo Simulations Studies, *Anal. Bioanal. Electrochem.*, 2018, **10**(10), p 1375–1398.
24. R. Hsissou, F. Benhiba, M. Khudhair, M. Berradi, A. Mahsoune, H. Oudda, A. El Harfi, I.B. Obot and A. Zarrouk, Investigation and Comparative Study of the Quantum Molecular Descriptors De-rived from the Theoretical Modeling and Monte Carlo Simulation of Two New Macromolecular Polyepoxide Architectures TGEEBA and HGEMDA, *J. King Saud Univ. Sci.*, 2020, **32**, p 667–676.
25. A. Kokalj, On the HSAB Based Estimate of Charge Transfer Between Adsorbates and Metal Surfaces, *Chem. Phys.*, 2012, **393**, p 1–12.
26. F. Benhiba, H. Serrar, R. Hsissou, A. Guenbour, A. Bellaouchou, M. Tabyaoui, S. Boukhris, H. Oudda, I. Warad and A. Zarrouk, Tetrahydropyrimido-Triazepine Derivatives as Anti-corrosion Additives for Acid Corrosion: Chemical, Electrochemical, Surface and Theoretical Studies, *Chem. Phys. Lett.*, 2020, **743**, p 137181.
27. Materials Studio, Revision 8.0, Accelrys Inc., San Diego, USA (2015)
28. H.C. Andersen, Molecular Dynamics Simulations at Constant Pressure and/or Temperature, *Chem. Phys.*, 1980, **72**, p 2384–2393.
29. H. Sun, COMPASS: An ab Initio Force-Field Optimized for Condensed-Phase Applications Overview with Details on Alkane and Benzene Compounds, *Phys. Chem. B*, 1998, **102**, p 7338–7364.
30. M. Rbaa, F. Benhiba, I.B. Obot, H. Oudda, I. Warad, B. Lakhrissi and A. Zarrouk, Two New 8-hydroxyquinoline Derivatives as an Efficient Corrosion Inhibitors for Mild Steel in Hydrochloric Acid: Synthesis, Electrochemical, Surface Morphological, UV– Visible and Theoretical Studies, *J. Mol. Liq.*, 2019, **276**, p 120–133.
31. B. Tan, S. Zhang, W. Li, X. Zuo, Y. Qiang, L. Xu, J. Hao and S. Chen, Experimental and Theoretical Studies on Inhibition Performance of Cu Corrosion in 0.5 M H_2SO_4 by Three Disulfide Derivatives, *J. Ind. Eng. Chem.*, 2019, **77**, p 449–460.
32. T.A. Salman, K.F. Al-Azawi, I.M. Mohammed, S.B. Al-Baghdadi, A.A. Al-Amiery, T.S. Gaaze and A.A.H. Kadhum, Experimental

Studies on Inhibition of Mild Steel Corrosion by Novel Synthesized Inhibitor Complemented with Quantum Chemical Calculations, *Results Phys.*, 2018, **10**, p 291–296.
33. F. Benhiba, Z. Benzekri, A. Guenbour, M. Tabyaoui, A. Bellaouchou, S. Boukhris, H. Oudda, I. Warad and A. Zarrouk, Combined Electronic/atomic Level Computational, Surface (SEM/EDS), Chemical and Electrochemical Studies of the Mild Steel Surface by Quinoxalines Derivatives Anti-corrosion Properties in 1 mol L^{-1} HCl Solution, *Chin. J. Chem. Eng.*, 2020, **28**, p 1436–1458.
34. Z. El Adnani, M. Mcharfi, M. Sfaira, A.T. Benjelloun, M. Benzakour, M. Ebn Touhami, B. Hammouti and M. Taleb, Investigation of Newly Pyridazine Derivatives as Corrosion Inhibitors in Molar Hydrochloric Acid. Part III: Computational Calculations, *Int. J. Electrochem. Sci.*, 2012, **7**, p 3982–3996.
35. R.G. Pearson, Absolute Electronegativity and Hardness: Application to Inorganic Chemistry, *Inorg. Chem.*, 1988, **27**, p 734–740.
36. A. Koulou, F. Benhiba, M. Rbaa, N. Errahmany, Y. Lakhrissi, R. Touir, B. Lakhrissi, A. Zarrouk and M.S. Elyoubi, Synthesis of New Epoxy Glucose Derivatives as Inhibitor for Mild Steel Corrosion in 1.0 M HCl: DMol3 Theory and Molecular Dynamics Simulation Study: Part-2, *Mor J Chem*, 2020, **8**(1), p 157–166.
37. M.M. Solomon, S.A. Umoren, I.I. Udosoro and A.P. Udoh, Inhibitive and Adsorption Behavior of Carboxymethyl Cellulose on Mild Steel Corrosion in H_2SO_4, *Corros. Sci.*, 2010, **52**, p 1317–1325.
38. A. Dell, D.H. William, H.R. Morris, G.A. Smith, J. Feeney and G.C.K. Roberts, Structure Revision of the Antibiotic Echinomycin, *J. Am. Chem. Soc.*, 1975, **97**, p 2497–2502.
39. H. Zarrok, S.S. Al-Deyab, A. Zarrouk, R. Salghi, B. Hammouti, H. Oudda, M. Bouachrine and F. Bentiss, Thermodynamic Characterisation and Density Functional Theory Investigation of 1,1',5,5'-Tetramethyl-1H, 1'H-3,3'- Bipyrazole as Corrosion Inhibitor of C38 Steel Corrosion in HCl, *Int. J. Electrochem. Sci.*, 2012, **7**, p 4047–4063.
40. K. Juttner, Electrochemical Impedance Spectroscopy (EIS) of Corrosion Processes on Inhomogeneous Surfaces, *Electrochim Acta*, 1990, **35**, p 1501–1508.
41. A.R.S. Priya, V.S. Muralidharam and A. Subramania, Development of Novel Acidizing Inhibitors for Carbon Steel Corrosion in 15% Boiling Hydrochloric Acid, *Corrosion*, 2008, **64**, p 541–552.
42. H. Zarrok, A. Zarrouk, B. Hammouti, R. Salghi, C. Jama and F. Bentiss, Corrosion Control of Carbon Steel in Phosphoric Acid by Purpald–Weight Loss, Electrochemical and XPS Studies, *Corros. Sci.*, 2012, **64**, p 243–252.
43. M. Izadi, I. Mohammadi, T. Shahrabi, B. Ramezanzadeh and A. Fateh, Corrosion Inhibition Performance of Novel Eco-friendly Nanoreservoirs as bi-component Active System on Mild Steel in Aqueous Chloride Solution, *J. Taiwan Inst. Chem. E*, 2019, **95**, p 555–568.
44. A. Popova, E. Sokolova, S. Raicheva and M. Christov, AC and DC Study of the Temperature Effect on Mild Steel Corrosion in Acid Media in the Presence of Benzimidazole Derivatives, *Corros Sci.*, 2003, **45**, p 33–58.
45. D. Daoud, T. Douadi, S. Issaadi and S. Chafaa, Adsorption and Corrosion Inhibition of New Synthesized Thiophene Schiff Base on Mild Steel X52 in HCl and H_2SO_4 Solutions, *Corros Sci.*, 2014, **79**, p 50–58.
46. M.S. Morad, Inhibition of Iron Corrosion in Acid Solutions by Cefatrexyl: Behaviour Near and at the Corrosion Potential, *Corros Sci.*, 2008, **50**, p 436–448.
47. M. Lebrini, F. Bentiss, N. Chihib, C. Jama, J.P. Hornez and M. Lagrenée, Polyphosphate Derivatives of Guanidine and Urea Copolymer: Inhibiting Corrosion Effect of Armco Iron in Acid Solution and Antibacterial Activity, *Corros Sci.*, 2008, **50**, p 2914–2918.
48. M. El Faydy, M. Galai, A. El Assyry, A. Tazouti, R. Touir, B. Lakhrissi, M. Ebn Touhami and A. Zarrouk, Experimental Investigation on the Corrosion Inhibition of Carbon Steel by 5-(chloromethyl)-8-quinolinol Hydrochloride in Hydrochloric Acid Solution, *J. Mol. Liq.*, 2016, **219**, p 396–404.
49. F.B. Growcock and R.J. Jasinski, Time-Resolved Impedance Spectroscopy of Mild Steel in Concentrated Hydrochloric Acid, *J Electrochem Soc.*, 1989, **136**, p 2310–2314.
50. Y. Kharbach, F.Z. Qachchachi, A. Haoudi, M. Tourabi, A. Zarrouk, C. Jama, L.O. Olasunkanmi, E.E. Ebenso and F. Bentiss, Anticorrosion Performance of Three Newly Synthesized Isatin Derivatives on Carbon Steel in Hydrochloric Acid Pickling Environment: Electrochemical, Surface and Theoretical Studies, *J Mol Liq*, 2017, **246**, p 302–316.
51. A.S. Fouda, A.F. Hassan, M.A. Elmorsi, T.A. Fayed and A. Abdelhakim, Chalcones as Environmentally-Friendly Corrosion Inhibitors for Stainless Steel Type 304 in 1M HCl Solutions, *Int. J. Electrochem. Sci.*, 2014, **9**, p 1298–1320.
52. M. Nasibi, M. Mohammady, E. Ghasemi, A. Ashrafi, D. Zaarei and G. Rashed, Corrosion Inhibition of Mild Steel by Nettle (Urtica dioica L.) Extract: Polarization, EIS, AFM, SEM and EDS Studies, *J. Adhes Sci. Technol.*, 2013, **27**, p 1873–1885.
53. S. Jyothi and J. Ravichandran, Inhibitive Action of the Acid Extract of Luffa Aegyptiaca Leaves on the Corrosion of Mild Steel in Acidic Medium, *J. Adhes Sci. Technol.*, 2015, **29**, p 207–231.
54. M. Rbaa, A.S. Abousalem, M.E. Touhami, I. Warad, F. Bentiss, B. Lakhrissi and A. Zarrouk, Novel Cu (II) and Zn (II) Complexes of 8-hydroxyquinoline Derivatives as Effective Corrosion Inhibitors for Mild Steel in 1.0 M HCl Solution: Computer Modeling Supported Experimental Studies, *J. Mol. Liq.*, 2019, **290**, p 111243.
55. T. Kamimura, S. Nasu, T. Tazaki, K. Kuzushita and S. Morimoto, Mössbauer Spectroscopic Study of Rust Formed on a Weathering Steel and a Mild Steel Exposed for a Long Term in an Industrial Environment, *Mater Trans.*, 2002, **43**, p 694–703.
56. F. Zhang, Y. Tang, Z. Cao, W. Jing, Z. Wu and Y. Chen, Performance and Theoretical Study on Corrosion Inhibition of 2-(4-pyridyl)-Benzimidazole for Mild Steel in Hydrochloric Acid, *Corros Sci.*, 2012, **61**, p 1–9.
57. F. Benhiba, H. Zarrok, A. Elmidaoui, M. El Hezzat, R. Touir, A. Guenbour, A. Zarrouk, S. Boukhris and H. Oudda, Theoretical Prediction and Experimental Study of 2-phenyl-1, 4-dihydroquinoxaline as a Novel Corrosion Inhibitor for Carbon Steel in 1.0 HCl, *J. Mater. Environ. Sci.*, 2015, **6**(8), p 2301–2314.
58. M.A. Chidiebere, C.E. Ogukwe, K.L. Oguzie, C.N. Eneh and E.E. Oguzie, corrosion Inhibition and Adsorption Behaviour of Punica Granatum Extract on Mild Steel in Acidic Environments: Experimental and Theoretical Studies, *Ind. Eng. Chem. Res.*, 2012, **51**, p 668–677.
59. L.C. Murulana, A.K. Singh, S.K. Shukla, M.M. Kabanda and E.E. Ebenso, Experimental and Quantum Chemical Studies of Some bis(trifluoromethyl-sulphonyl)imide imidazolium-based Ionic Liquids as Corrosion Inhibitors for Mild Steel in Hydrochloric Acid Solution, *Ind. Eng. Chem. Res.*, 2012, **51**, p 13282–13299.
60. V.S. Sastri and J.R. Perumareddi, Molecular Orbital Theoretical Studies of Some Organic Corrosion Inhibitors, *Corrosion*, 1997, **53**, p 617–622.
61. Y. Tang, X. Yang, W. Yang, R. Wan, Y. Chen and X. Yin, A preliminary Investigation of Corrosion Inhibition of Mild Steel in 0.5M H_2SO_4 by 2-amino-5-(n-pyridyl)-1,3,4- thiadiazole: Polarization, EIS and Molecular Dynamics Simulations, *Corros Sci.*, 2010, **52**, p 1801–1808.
62. H. Rahmani, K.I. Alaoui, M. EL Azzouzi, F. Benhiba, A. El Hallaoui, Z. Rais, M. Taleb, A. Saady, B. Labriti, A. Aouniti and A. Zarrouk, Corrosion Assessement of Mild Steel in Acid Environment using Novel Triazole Derivative as a Anti-corrosion Agent: A Combined Experimental and Quantum Chemical Study, *Chem. Data Collect*, 2019, **24**, p 100302.
63. Z. Rouifi, F. Benhiba, M. El Faydy, T. Laabaissi, H. About, H. Oudda, I. Warad, A. Guenbour, B. Lakhrissi and A. Zarrouk, Performance and Computational Studies of New Soluble Triazole as Corrosion Inhibitor for Carbon Steel in HCl, *Chem. Data Collect*, 2019, **22**, p 100242.
64. M. El Hezzat, M. Assouag, H. Zarrok, Z. Benzekri, A. El Assyry, S. Boukhris, A. Souizi, M. Galai, R. Touir, M. Ebn Touhami, H. Oudda and A. Zarrouk, Correlated DFT and Electrochemical Study on Inhibition Behavior of Ethyl 6-amino-5-cyano-2-methyl-4-(p-tolyl)-4H-pyran-3-carboxylate for the Corrosion of Mild Steel in HCl, *Der Pharma Chem.*, 2015, **7**(10), p 77–88.
65. E.E. Oguzie, C.B. Adindu, C.K. Enenebeaku, C.E. Ogukwe, M.A. Chidiebere and K.L. Oguzie, Natural Products for Material Protection: Mechanism of Corrosion Inhibition of Mild Steel by Acid Extracts of Piper Guineense, *J. Phys. Chem. C*, 2012, **116**, p 13603–13615.
66. N.O. Obi-Egbedi and I.B. Obot, Inhibitive Properties, Thermodynamic and Quantum Chemical Studies of Alloxazine on Mild Steel Corrosion in H_2SO_4, *Corros Sci.*, 2011, **53**, p 263–275.
67. A. Dehghani, G. Bahlakeh and B. Ramezanzadeh, A Detailed Electrochemical/theoretical Exploration of the Aqueous Chinese Gooseberry Fruit Shell Extract as a Green and Cheap Corrosion Inhibitor for Mild Steel in Acidic Solution, *J. Mol. Liq.*, 2019, **282**, p 366–384.

68. M. Khattabi, F. Benhiba, S. Tabti, A. Djedouani, A. El Assyry, R. Touzani, I. Warad, H. Oudda and A. Zarrouk, Performance and Computational Studies of Two Soluble Pyran Derivatives as Corrosion Inhibitors for Mild Steel in HCl, *J. Mol. Struct.*, 2019, **1196**, p 231–244.
69. MarvinSketch Software, Version: 18.22, ChemAxon Ltd., 2018
70. L. Zhou, Y. Lv, Y. Hu, J. Zhao, X. Xia and X. Li, Experimental and Theoretical Investigations of 1,3,5-tris(4-aminophenoxy)benzene as an Effective Corrosion Inhibitor for Mild Steel in 1 M HCl, *J. Mol. Liq.*, 2018, **249**, p 179–187.
71. M.M. Kabanda, L.C. Murulana, M. Ozcan, F. Karadag, I. Dehri, I.B. Obot and E.E. Ebenso, Quantum Chemical Studies on the corrosion inhibition of mild Steel by Some Triazoles and Benzimidazole Derivatives in Acidic Medium, *Int. J. Electrochem. Sci.*, 2012, **7**, p 5035–5056.
72. R.R. Contreras, P. Fuentealba, M. Galvan and P. Perez, A Direct Evaluation of Regional Fukui Functions in Molecules, *Chem. Phys. Lett.*, 1999, **304**, p 405–413.
73. R. Hsissou, O. Dagdag, S. Abbout, F. Benhiba, M. Berradi, M. El Bouchti, A. Berisha, N. Hajjaji and A. Elharfi, Novel Derivative Epoxy Resin TGETET as a Corrosion Inhibition of E24 Carbon Steel in 1.0M HCl Solution. Experimental and Computational (DFT and MD Simulations) Methods, *J. Mol. Liq.*, 2019, **284**, p 182–192.
74. G. Vengatesh and M. Sundaravadivelu, Non-toxicbisacodyl as an Effective Corrosion Inhibitor for Mild Steel in 1 M HCl: Thermodynamic Electrochemical SEM EDX AFM FT-IR DFT and Molecular Dynamics Simulation Studies, *J. Mol. Liq.*, 2019, **287**, p 110906.
75. L. Guo, S. Kaya, I.B. Obot, X. Zheng and Y. Qiang, Toward Understanding the Anticorrosive Mechanism of Some Thiourea Derivatives for Carbon Steel Corrosion: A Combined DFT and Molecular Dynamics Investigation, *J. Colloid Interface Sci.*, 2017, **506**, p 478–485.
76. H. Kuhn and H. Rehage, The Molecular Structure of Sodium Octanoate Micelles Studied by Molecular Dynamics Computer Experiments, *Ber Bunsenges J Phys Chem*, 1997, **101**(10), p 1485–1492.
77. N. Asadi, M. Ramezanzadeh, G. Bahlakeh and B. Ramezanzadeh, Utilizing Lemon Balm Extract as an Effective Green Corrosion Inhibitor for Mild Steel in 1M HCl Solution: A Detailed Experimental, Molecular Dynamics, Monte Carlo and Quantum Mechanics Study, *J. Taiwan Inst. Chem. E*, 2019, **95**, p 252–272.
78. A. Elyaktini, A. Lachiri, M. Elfaydy, F. Benhiba, H. Zarrok, M. Elazzouzi, M. Zertoubi, M. Azzi, B. Lakhrissi and A. Zarrouk, Inhibitor Effect of New Azomethine Derivative Containing an 8-hydroxyquinoline Moiety on Corrosion Behavior of Mild Carbon Steel in Acidic Media, *Int. J. Corros Sca Inhib.*, 2018, **7**(4), p 609–632.
79. M.N. El-Haddad and K.M. Elattar, Synthesis, Characterization and Inhibition Effect of New Antipyrinyl Derivatives on Mild Steel Corrosion in Acidic Solution, *Int. J. Ind. Chem.*, 2015, **6**, p 105–117.
80. M. Yadav, R.R. Sinha, S. Kumar and T.K. Sarkar, Corrosion inhibition Effect of Spiropyrimidinethiones on Mild Steel in 15% HCl Solution: Insight from Electrochemical and Quantum Studies, *RSC Adv.*, 2015, **5**, p 70832–70848.